BIOCHEMICAL PHARMACOLOGY 75 (2008) 1161–1169

available at www.sciencedirect.com

ScienceDirect

journal homepage: www.elsevier.com/locate/biochempharm

Molecular basis for the interaction of four different classes of substrates and inhibitors with human aromatase

Yanyan Hong, Michael Cho, Yate-Ching Yuan, Shiuan Chen *

Department of Surgical Research and Division of Information Sciences, Beckman Research Institute of the City of Hope, 1500 E. Duarte Road, Duarte, CA 91010, United States

ARTICLE INFO

Article history:
Received 2 October 2007
Accepted 19 November 2007

Keywords:
Aromatase inhibitor
Estrogen
Cytochrome P450
Mutagenesis
Structural model

ABSTRACT

Aromatase cytochrome P450 (CYP19) converts androgen to estrogen. In this study, the interactions of four classes of compounds, 17β-estradiol (the product of aromatase), 17-methyltestosterone (a synthetic androgen), dibenzylfluorescein (a synthetic substrate of aromatase), and coumestrol (a phytoestrogen), with aromatase were investigated through spectral analysis using purified human recombinant aromatase and site-directed mutagenesis studies using CHO cells expressing wild-type human aromatase or five aromatase mutants, E302D, D309A, T310S, S478T and H480Q. Spectral analysis showed that a type I binding spectrum was produced by the binding of 17-methyltestosterone to aromatase and a novel binding spectrum of aromatase was induced by dibenzylfluorescein. Mutagenesis experiments demonstrated that residues S478 and H480 in the β-4 sheet play an important role in the binding of all four compounds. Computer-assisted docking of these compounds into the three-dimensional model of aromatase revealed that: (1) weak interaction between 17β-estradiol and the β-4 sheet of aromatase facilitates the release of 17β-estradiol from the active site of aromatase; (2) 17-methyl group of 17-methyltestosterone affects its binding to aromatase; (3) dibenzylfluorescein binds to the active site of aromatase with its O-dealkylation site near the heme iron and residue T310; and (4) coumestrol binds to aromatase in a manner such that rings A and C of coumestrol mimic rings A and B of steroid. These structure–function studies help us to evaluate the structural model of aromatase, and to accelerate the structure-based design for new aromatase inhibitors.

1. Introduction

The female hormone, estrogen, plays an important role in breast cancer development. Upon binding to estrogen, estrogen receptor (ER) activates transcription of its target genes, which are responsible for cancer cell proliferation in estrogen-dependent breast tumor. The most important estrogens in humans are estrone (E1) and 17β-estradiol (E2), which are synthesized from androstenedione and testosterone, respectively, by aromatase cytochrome P450 (CYP19) enzyme. The third-generation aromatase inhibitors (AIs), which include two triazole derivatives, anastrozole (Arimidex) [1] and letrozole (Femara) [2], and one steroid analogue, exemestane (Aromasin) [3], are currently used clinically for the treatment of hormone-dependent breast cancer in postmenopausal women [4–7].

* *Corresponding author*. Tel.: +1 626 256 4673 63454; fax: +1 626 301 8972.
E-mail address: schen@coh.org (S. Chen).

Abbreviations: E1, estrone; E2, 17β-estradiol; CYP, cytochrome P450; AIs, aromatase inhibitors; 3-D, three-dimensional; 17MT, 17-methyltestosterone; DBF, dibenzylfluorescein; WT, wild-type; CHO, Chinese hamster ovarian; 17ME2, 17-methylestradiol; ER, estrogen receptor; IC_{50}, 50% inhibitory concentration.

0006-2952/$ – see front matter © 2007 Published by Elsevier Inc.
doi:10.1016/j.bcp.2007.11.010

The structure–function characterization of aromatase would provide useful information for the understanding of the reaction mechanisms of the enzyme and for the design of new potent AIs. However, the structural basis of drug binding to aromatase is not well understood because the three-dimensional (3-D) crystal structure of aromatase is unknown. Previous studies from our laboratory and others have made considerable progress towards characterizing the structure–function relationship of aromatase [8–14]. Recently, a theoretical 3-D model of aromatase (PDB code 1TQA) was built based on the crystal structure resolved at 2.55 Å of warfarin-bound human CYP2C9 [14]. We have proposed a new clamping mechanism of androstenedione and exemestane binding to the active site of aromatase, based on the results from site-directed mutagenesis, proteomic analysis, and computer-assisted protein–ligand docking using the 3-D model of aromatase [15]. This clamping mechanism provides insight into the interaction of aromatase with its steroidal ligands.

In this study we investigated the interaction of aromatase with four classes of compounds, E2, 17-methyltestosterone (17MT), dibenzylfluorescein (DBF), and coumestrol, each having its own unique structural features (Fig. 1). E2, the aromatization product of testosterone by aromatase, has the same steroid scaffold as testosterone. The major structural difference between E2 and testosterone is that E2 has a planar aromatic A ring, while testosterone has a non-aromatic six-carbon A ring. In a recent publication [15], we discussed how the androgen substrate binds to aromatase and how the aromatization reaction occurs; however, how this structural conversion by the aromatization reaction leads to the release of E2 from aromatase remains a mystery. 17MT is a synthetic androgen used to treat men with a testosterone deficiency. It is also used as a component in contraceptive. 17MT has an extra 17 alpha-methyl group compared to androstenedione and testosterone, whereas this 17 alpha-methyl makes it a poor substrate of aromatase [16]. DBF is a fluorescein derivative and a substrate for CYP enzymes, such as CYP3A4, CYP2C8, and aromatase. The benzyl ether group at position 6 of DBF (as shown in Fig. 1) can be O-dealkylated by CYP enzymes [17]. DBF is an effective substrate for aromatase. The relatively large molecular size of DBF when compared to the steroidal substrates of aromatase leads us to question how DBF binds to the active site of aromatase. Coumestrol, a phytoestrogen, has a similar structural scaffold to a steroid. It is a potent antagonist for ER; however, it was found to be a weak competitive inhibitor of aromatase [18].

These four compounds contain special structural characters. The structure–function characterization of aromatase in this study helps us to examine the accuracy of the predicted active site pocket of aromatase and the hypothetical clamping mechanism of ligand binding.

2. Materials and methods

2.1. Chemicals

G418 and fetal bovine serum were purchased from Omega Scientific (Tarzana, CA); Ham's F-12 medium was purchased from BioWhittaker (Walkersville, MD); Hepes buffer was purchased from Irvine Scientific (Santa Ana, CA); sodium pyruvate, L-glutamine, and penicillin-streptomycin were purchased from Cellgro Mediatech (Herndon, VA); [1β-^{3}H] androstenedione was purchased from PerkinElmer (Boston, MA); 17MT, E2, DBF, and coumestrol were purchased from Sigma–Aldrich Co. (Saint Louis, MO); letrozole was provided by Novartis Pharmaceuticals Corporation (East Hanover, NJ). All inhibitor stock solutions were prepared in 100% ethanol: 50 mM E2, 100 mM 17MT, 5 mM DBF, 2 mM coumestrol, and 17 mM letrozole.

2.2. Cell line

The aromatase-overexpressing Chinese hamster ovarian (CHO) cell line was prepared by stable transfection with the human placental aromatase gene and G418 selection, as previously described [19]. Cells were maintained with Ham's F-12 medium with 15 mM Hepes buffer, 1 mM sodium pyruvate,

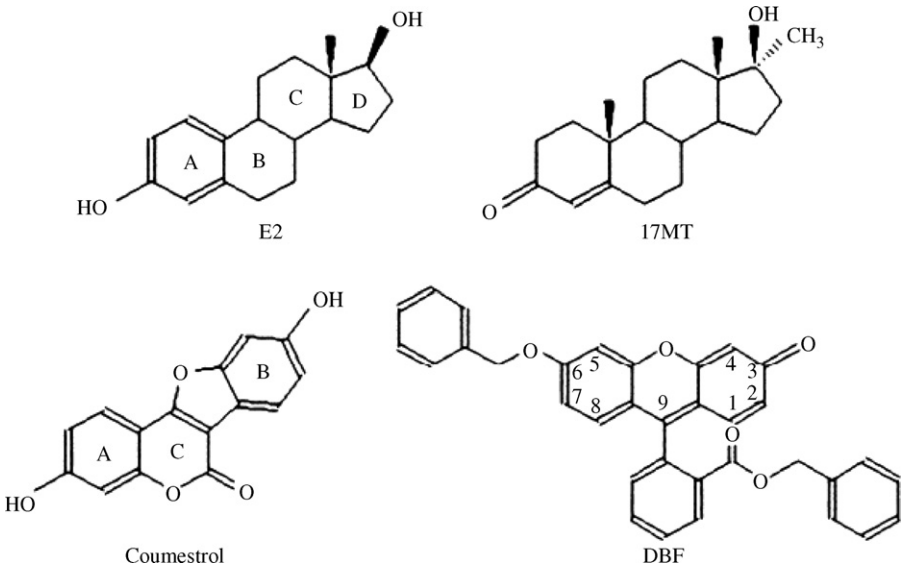

Fig. 1 – Chemical structures of E2, 17MT, coumestrol, and DBF.

2 mM L-glutamine, 10% fetal bovine serum, and a mixture of antibodies: 1% penicillin-streptomycin and 1 mg/ml G418.

2.3. Site-directed mutagenesis

The mutant cDNAs were generated by the QuikChange site-directed mutagenesis kit (Stratagene, La Jolla, CA) using the WT aromatase expression plasmid pHβ-Aro [20] as template, then transformed into DH5α cells. All mutations were verified by DNA sequencing. For stable transfections, mutant plasmids were transfected into CHO cells using lipofectin (Life Technologies, Inc., Rockville, MD). After 2 weeks of G418 selection, transfected cells were maintained in media containing 600 μg/ml G418.

2.4. In-cell aromatase activity assay

Aromatase activity was determined using the tritiated water-release method [21]. Aromatase-transfected CHO cells were seeded in six-well plates, and 1 ml of serum-free media containing both 100 nM [1β-^{3}H] androstenedione and 1 μM progesterone were added to each well. After incubation at 37 °C for 1 h, the reaction was mixed with dextran-coated charcoal to remove trace amounts of unreacted substrate. After centrifugation at 13,000 rpm for 7 min, 300 μl of liberated tritiated water in the supernatant that was released during aromatization was added to 3 ml of scintillation liquid, and counted with a liquid scintillation counter (LS-6500, Beckman Coulter, Inc., Fullerton, CA). To determine protein concentration, the remaining cells in each well were solubilized with 0.5 M NaOH and analyzed using the Bradford assay [22].

2.5. Inhibition profile analysis

Inhibitors were included during the 1 h incubation of the aromatase activity assay. Since these compounds are competitive inhibitors with respect to the androgen substrate, K_i values for the inhibitors in WT aromatase or aromatase mutants were determined by Dixon plots ($1/\upsilon$ vs. [I]), generated with the average values of triplicate assays for each data point. Substrate [1β-^{3}H] androstenedione concentrations ranged from 16 to 200 nM. E2 and coumestrol concentrations ranged from 0 to 30 μM. DBF concentrations ranged from 0 to 0.6 μM. 17 MT concentrations ranged from 0 to 1 μM.

2.6. UV–visible spectral analysis

Purified recombinant human aromatase [15] was diluted to a concentration of 100 μg/ml with buffer A (50 mM potassium phosphate, pH 7.4, 20% glycerol) in 2 ml, and equally divided into two methacrylate cuvettes. After a baseline correction with these two cuvettes in a dual beam recording UV-1700 PharmaSpec UV–Vis Spectrophotometer (Shimadzu Scientific Instruments, Columbia, MD) from 700 nm to 350 nm, 0.2 mM 17MT, 0.1 mM E2, or 5 μM letrozole was added to the sample cuvet, stirred, and the difference spectra were recorded. The absorption spectra of 100 μg/ml ligand-free aromatase, 10 μM coumestrol, 12.5 μM DBF, and 100 μg/ml aromatase with 12.5 μM DBF were recorded after baseline correction with buffer A.

2.7. Computer-assisted docking

3-D structural model of aromatase (PDB code: 1TQA) [14] was selected for structure-based docking. 3-D structure of E2, 17MT, DBF and coumestrol were built by SYBYL (Tripos, St. Louis, MO). Computer-assisted docking was performed by Surflex-Dock (Tripos, St. Louis, MO). Androstenedione-binding pocket described in Hong et al. [15] was defined for ligand-based protomol generation for the docking of E2, 17MT, and coumestrol. Automatic protomol generation was selected for the docking of DBF.

3. Results

3.1. Interaction of E2 with aromatase

The structure of E2 differs from testosterone in the A ring, which is a planar aromatic ring with a hydroxyl group attached at carbon 3 (C-3), instead of a non-aromatic six-carbon ring with a keto group at C-3. In addition, the C-19 methyl group of testosterone is removed during the aromatization reaction. The structural conversion probably makes E2 a weaker ligand for aromatase than testosterone, and leads to the release of E2 from the active site of aromatase.

To investigate the molecular basis for the binding of E2 to the active site of aromatase, we determined the K_i (inhibitor dissociation constant) values for E2 inhibition of androstenedione aromatization in CHO cells transfected with WT human aromatase or five aromatase mutants, E302D, D309A, T310S, S478T, and H480Q. These five residues are thought to be present in the active site pocket of aromatase and play critical roles for the binding of androstenedione and exemestane [11,13,15,23]. Estimates of K_i were obtained from Dixon plots. A graphical illustration of this plot is presented in Fig. 2. The point of intersection of these pairs of lines represents the value of K_i. As expected, E2, a weak competitive inhibitor of aromatase, had a high K_i value (i.e., 4.73 μM), which indicates E2 has low binding affinity to aromatase. The S478T mutant significantly increased the binding affinity of E2 (Fig. 3A), which suggests the beta-4 sheet of aromatase plays an important role in E2 binding.

The UV–visible absorbance spectrum of aromatase induced by its ligand is associated with ligand-binding type. The UV–visible absorbance spectrum of CYP is associated with the coordinate state of the heme iron. In the six-coordinated state, the heme iron exists as a low spin state, in which the heme iron exhibits absorbance maximum at near 420 nm. While in the five-coordinated state, the heme iron exists as a high-spin state, in which the heme iron exhibits maximum at about 390 nm. Ligand-free aromatase showed an absorbance peak at approximately 420 nm (Fig. 4A), which is associated with the low spin heme iron, with a water molecule coordinated in the 6th position of the heme iron. To date, there are three types of ligand binding spectra of P450s [24,25]. To study the binding characteristics of E2, the UV–visible absorbance of the mixture of E2 and purified human recombinant aromatase were recorded. However, there were no spectral changes for the aromatase–E2 mixture when compared to the spectrum for

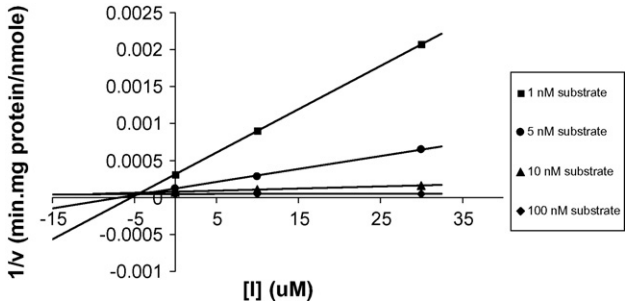

Fig. 2 – Dixon plot of reciprocal rates of aromatization (1/*v*) of WT human aromatase as a function of E2 concentration [*I*]. Each line represents linear regression analysis of reciprocal of average rates of aromatization for different substrate concentrations as a function of E2 concentration. Substrate concentrations: 1 nM (■), 5 nM (●), 10 nM (▲), and 100 nM (◆).

ligand-free aromatase. This indicates the binding of E2 to aromatase does not affect the spin state of the heme iron, probably due to the low binding affinity of E2 to the active site of aromatase.

To better understand the structural basis for the interaction between E2 and aromatase, E2 was docked into the androstenedione-binding pocket in the 3-D model of aromatase as described in Hong et al. [15] by means of Surflex-Dock (Tripos, St. Louis, MO). The docking orientation of E2 similar to that of androstenedione in Hong et al. was chosen. In the current model of the aromatase–E2 complex (Fig. 5A), E2 is localized high above the heme group, due to the removal of the C-19 methyl group of testosterone.

3.2. *Interaction of 17MT with aromatase*

17MT, a synthetic, exogenous androgen, has been widely used for hormone replacement therapy. 17MT also affects estrogen formation by inhibiting aromatase activity in a dose-dependent manner [26]. Thus, as a functional androgen and an orally active inhibitor of aromatase, 17MT may offer therapeutic potential for the prevention and treatment of hormone-dependent breast cancer.

The K_i values for 17MT inhibition of androstenedione aromatization in WT human aromatase and four aromatase mutants were determined (Fig. 3B). 17MT had a low binding affinity for aromatase, with a K_i value of 0.60 μM in WT aromatase, approximately 10–20 times the K_m values of androstenedione [11]. Mutants S478T and H480Q increased the binding affinity of 17MT, whereas mutants E302D and T310S did not significantly affect the binding affinity of 17MT in this study.

UV–visible spectral analysis was used to identify the binding property of 17MT to aromatase. Aromatase–17MT mixture had a type I difference spectrum, which was characterized by an absorbance reduction at 420 nm and an absorbance peak at around 390 nm (Fig. 4B). Type I binding spectrum is associated with the binding of substrates or substrate-like inhibitors, and is indicative of the high-spin, five-coordinated heme iron, which suggests that 17MT binds to the substrate-binding site. As a control, type II difference spectrum of aromatase was induced by letrozole, identified by an absorbance increase at 424 nm and a corresponding reduction at 390 nm (Fig. 4C). Type II binding spectrum is associated with the interaction of inhibitors which coordinate to the heme iron, and is corrected with a low-spin, six-coordinated state of the heme iron.

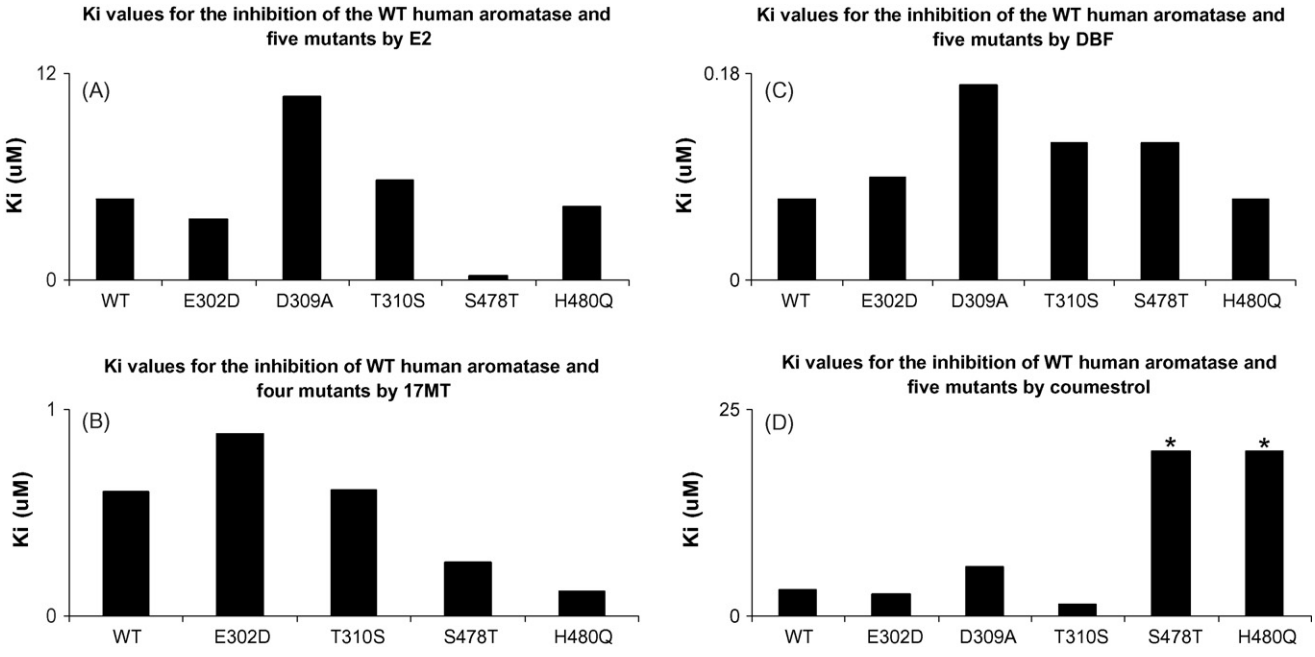

Fig. 3 – K_i values for the inhibition of the WT human aromatase and five mutants by E2, 17MT, DBF, and coumestrol. *Estimated K_i value due to the low solubility of coumestrol.

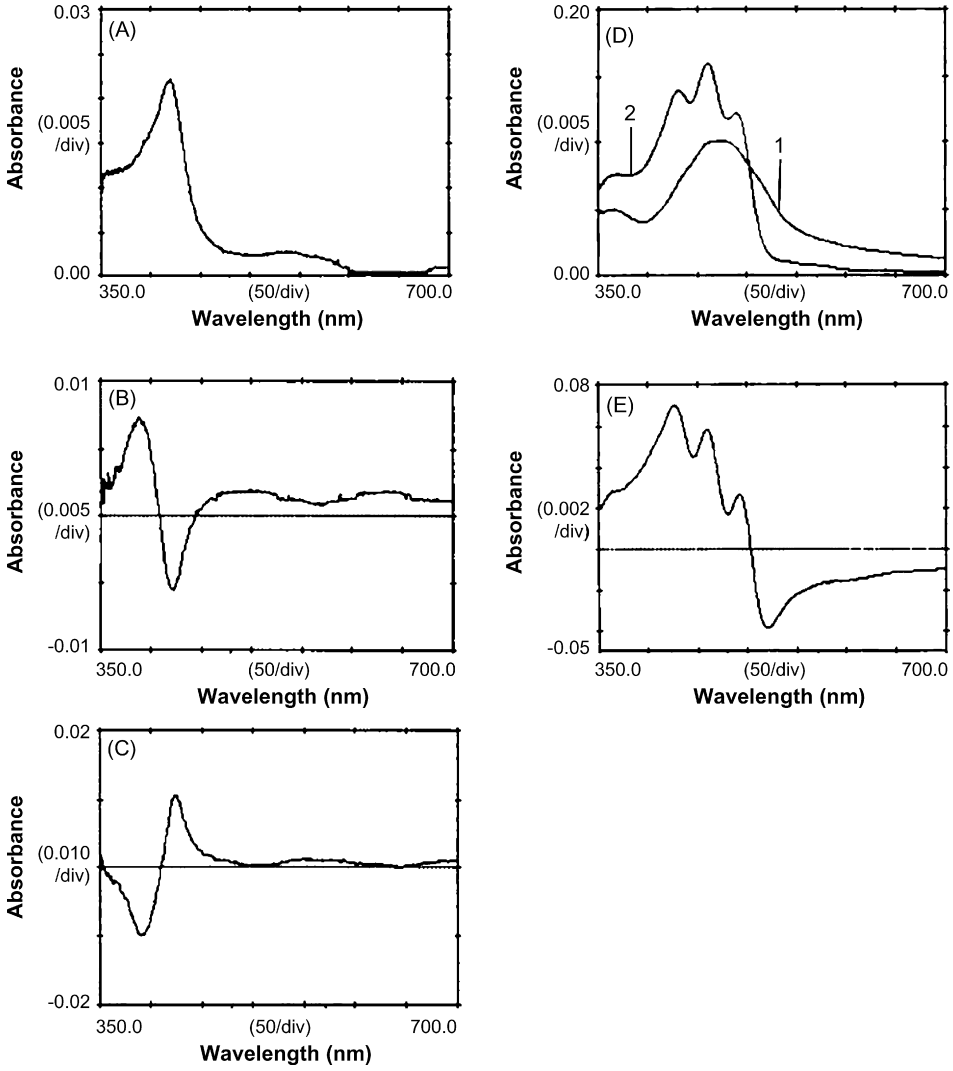

Fig. 4 – Ligand-induced absorbance spectra of aromatase. (A) UV–visible absorbance spectrum of ligand-free purified recombinant aromatase. (B) Type I binding spectrum was produced in the aromatase–17MT mixture. (C) Type II binding spectrum was produced in the aromatase–letrozole mixture. (D) 1: UV–visible absorbance spectrum of DBF; 2: UV–visible absorbance spectrum of the aromatase–DBF mixture. (E) Difference spectrum of the absorbance of the aromatase–DBF mixture minus that of DBF.

When compared to natural androgens, 17MT has an additional 17 alpha-methyl group. It is interesting to determine how this extra methyl group makes it a poor substrate. 17MT was docked into the androstenedione-binding pocket as described in Hong et al. [15] by Surflex-Dock. 17MT is located above the heme with its C-19 methyl group pointing to the iron, and is positioned next to I helix (Fig. 5B). The additional methyl group of 17MT may contribute to additional contacts with the B′ and F helices of aromatase, particularly at residues C124, D222, and A226.

3.3. *Binding of DBF in the active site of aromatase*

The large compound DBF has been shown to be an effective substrate for aromatase [17]. Following the O-dealkylation at position 6 of DBF by P450 enzymes, including aromatase, the resulting product can be converted to fluorescein through ester hydrolysis. Thus, a fluorometric assay using DBF substrate offers a potential approach to screen for aromatase inhibitors [17,27]. It is unclear how this large molecule, with a molecular mass of 512.6 Da, binds to the active site of aromatase.

Our site-directed mutagenesis experiments showed DBF had high binding affinity to aromatase, and five mutants, E302D, D309A, T310S, S478T and H480Q, did not significantly affect the binding affinity of DBF (Fig. 3C). UV–visible spectral analysis was used to determine the binding characteristics of DBF. Because DBF has broad absorbance between 400 and 550 nm (Fig. 4D), the difference spectrum of the absorbance of the aromatase–DBF mixture minus that of DBF were recorded (Fig. 4E). This DBF-binding spectrum of aromatase, characterized by three absorbance peaks (430, 460, and 490 nm), does not match three previously identified types of ligand binding spectra of CYPs [24,25], which indicates that DBF may bind to

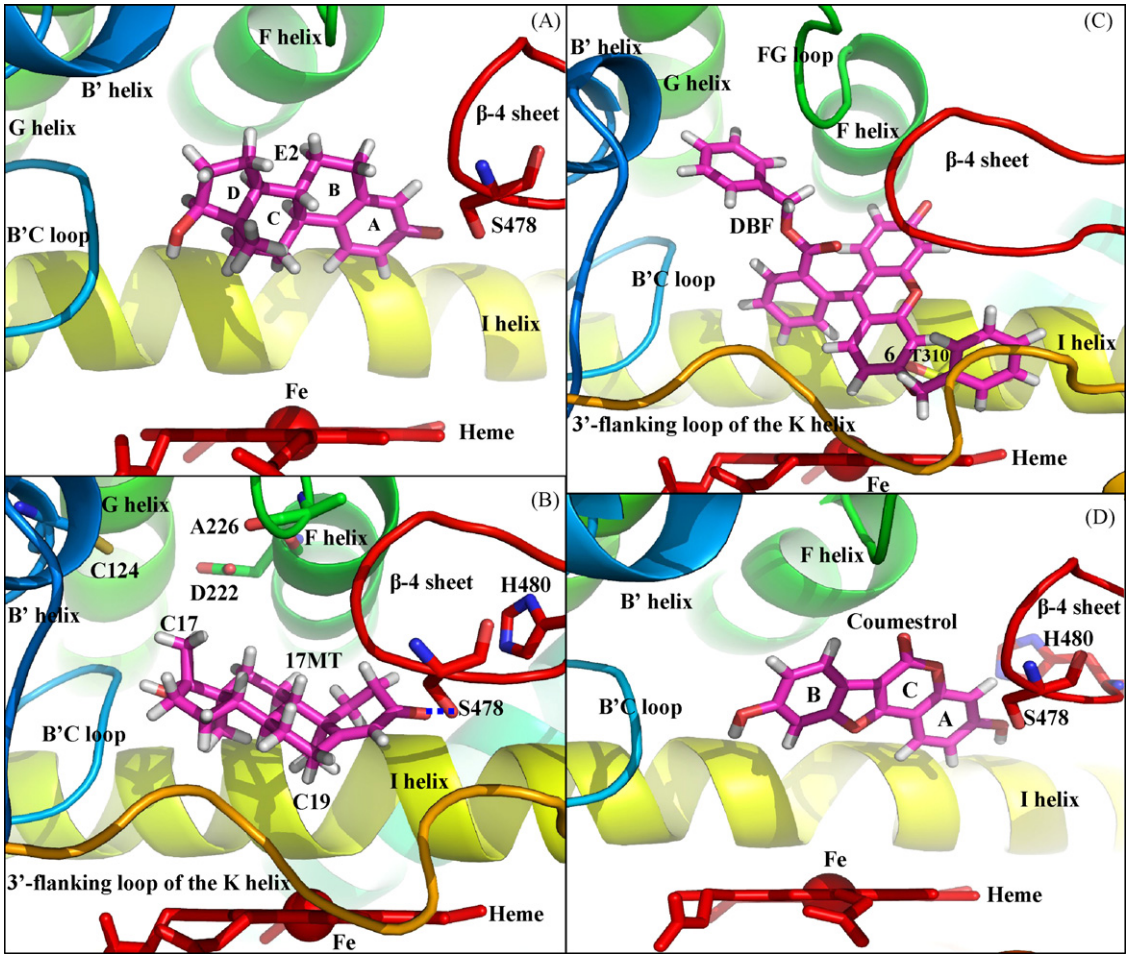

Fig. 5 – Docking of E2, 17MT, DBF, and coumestrol in the active site of the 3-D model of aromatase. Ligands are shown in *purple* above the heme group (colored in *red*). (A) The docking model of the aromatase–E2 complex. (B) The docking model of the aromatase–17MT complex. (C) The docking model of the aromatase–DBF complex. (D) The docking model of the aromatase–coumestrol complex. The heme iron is shown in *sphere* representation. The 3-D model of aromatase is displayed as *secondary structure cartoon* and colored according to sequence succession from *blue* to *red*. Helices B′, F, G, and I are displayed as *helical structures*. The B′C loop, FG loop, 3′-flanking loop of the K helix, and the β-4 sheet are displayed as *loop structures*. Amino acid side chains are shown in *stick* representation. Oxygen atoms are colored in *red*, nitrogen in *blue*, sulfur in *yellow*, hydrogen in *white*. The *blue dashed line* is drawn between the atoms involved in a hydrogen bond.

aromatase in a novel manner. The exact nature of the interaction between DBF and aromatase is unknown.

Computer-assisted molecular docking was used to elucidate how this large molecule binds to aromatase. When we used automatic protomol generation in Surflex-Dock, DBF fits into the active site of aromatase with its O-dealkylation site (i.e., position 6 of DBF) near the iron and residue T310 (Fig. 5C). The docking orientation of DBF is supported by the report that demonstrated the dioxygen activation mediated by the conserved threonine (T310 in aromatase) is required for the O-dealkylation reaction [28]. There are 33 amino acids in the aromatase active site that are 5 Å from DBF in the docking complex. Besides those residues involved in the binding of steroids, there are more residues, which are located at the B′, F, and G helices, FG loop, and the 3′-flanking loop of the K helix, involved in the binding of DBF.

3.4. *Inhibition of aromatase by coumestrol*

Coumestrol is a phytoestrogen that occurs naturally in soybean and forage crops. Phytoestrogens are plant chemicals that exhibit structural and functional similarity to estrogen. Some phytoestrogens may play a beneficial role in preventing breast cancer by competing with estrogen for binding to ER, and decreasing estrogen levels through inhibiting aromatase activity. Coumestrol is a strong antagonist for ER, but is a weak competitive inhibitor for aromatase [18]. The study of aromatase–coumestrol interaction will help us to better understand why this planar, estrogen-like molecule is a weak inhibitor for aromatase.

The site-directed mutagenesis experiments showed that coumestrol had a high K_i value in WT aromatase, as expected for a weak inhibitor (Fig. 3D). Mutants S478T and H480Q greatly

decreased the binding affinity of coumestrol to aromatase, whereas there were no significant effects on the binding of coumestrol to the E302D, D309A and T310S mutants. Our results indicate that active site residues S478 and H480 are involved in coumestrol binding, which suggests coumestrol binds to the active site pocket of aromatase. UV–visible spectral analysis was used to determine the binding characteristics of coumestrol. However, strong UV absorbance of coumestrol prevented us from analyzing the UV–visible absorbance of the aromatase–coumestrol mixture.

To better understand how this planar molecule binds to aromatase, we docked coumestrol into the active site of aromatase by Surflex-Dock. Due to its small size, several different docked poses may be reasonable, and thus it is difficult to determine the orientation of coumestrol in the active site of aromatase. Because of the structural similarity between E2 and coumestrol, we thought that rings A and C of coumestrol might mimic rings A and B of E2. The assumption that rings A and C of coumestrol mimic rings A and B of E2 was also used in a previous study about the interaction of aromatase and flavones [23]. The docked complex based on this assumption is shown in Fig. 5D. Furthermore, due to the planar structure and small size of the coumestrol molecule, coumestrol enters deep into the cleft between I helix and beta-4 sheet, which results in close contacts between coumestrol and residues S478 and H480.

4. Discussion

The structure difference between androgen and estrogen is in the A ring. The fact that this structural conversion causes dramatically different binding affinity between androgen and estrogen leads us to propose that the beta-4 sheet, which is near the A ring from our structural model, must play an important role in steroid binding. The beta-4 sheet of aromatase was thought to play important roles in the clamping mechanism for steroidal substrate binding [15]. Residue S478, located at the beta-4 sheet of aromatase, was hypothesized to form a hydrogen bond with the keto group at C-3 of androstenedione, and was thought to be involved in the aromatization reaction [15]. The present study demonstrated that residue S478 is also involved in E2 binding to aromatase: site-directed mutagenesis experiments showed that the S478T mutant increased the binding affinity of E2. However, the planar aromatic A ring of E2 probably has weaker interaction with the beta-4 sheet when compared to the non-aromatic six-carbon A ring of substrate, and leads to the release of E2 from the active site of aromatase. In addition, our docking model showed that E2 is localized high above the heme group, which may leave extra space allowing a water molecule to re-ligate to the iron. The re-ligation of a water molecule to the heme iron following the removal of the C-19 methyl group of testosterone may also trigger the release of E2 from the active site.

The mutagenesis studies also demonstrated the importance of the beta-4 sheet on 17MT binding: mutants S478T and H480Q increase the binding affinity of 17MT. In the current model of the aromatase–17MT complex, residues S478 and H480 are located near the A ring of 17MT. Residue S478 forms a hydrogen bond with the C-3 keto oxygen of 17MT. The larger side chain of the mutant threonine (at position 478) may form stronger interaction with 17MT. The replacement of a histidine residue at position 480 with a glutamine may stabilize 17MT through the formation of an additional hydrogen bond between the glutamine and the C-3 keto oxygen of 17MT. Furthermore, our docking model of the aromatase–17MT complex reveals additional contacts between the 17-methyl group of 17MT and the B′ and F helices of aromatase. However, these additional contacts may cause steric clash, thereby reducing the stability of 17MT in the active site of aromatase.

UV–visible spectral analysis using purified recombinant human aromatase revealed a novel spectrum of aromatase upon binding of DBF, with three absorbance peaks at 430, 460, and 490 nm. Absorbance peaks at 430 and 460 nm may reflect a type III binding. Type III binding spectrum is characterized by two absorbance maxima at 425–430 and 455–460 nm. The nature of type III binding has not been elucidated. It has been proposed that the absorbance at 425–430 nm of type III binding spectrum could result from a shift in the spin state of the heme iron or from a stretching of the iron–thiolate bond [29–31]. While the 455–460 nm peak is usually considered to reflect the interaction of carbene, an uncharged reactive intermediate, with the iron [30]. Therefore, the 455–460 nm peak of type III binding spectrum is thought to reflect the formation of P450 metabolic–intermediate complex [30,32–34]. We observed this novel binding spectrum in the aromatase–DBF complex in the absence of NADPH-P450 reductase and NADPH. The 430 nm peak could result from a stretching of the iron–thiolate bond induced by the interaction of DBF with aromatase in the vicinity of heme. In the absence of NADPH-P450 reductase and NADPH, it is unclear whether the 460 nm peak is from the aromatase metabolic–intermediate complex. This binding spectrum for DBF suggests that DBF interacts with the heme iron, and binds to the active site in a novel manner. Our docking model indicates that strong interaction between aromatase and DBF (i.e., low K_i of DBF) may result from their extensive contacts. We did not detect significant changes in the K_i values in the E302D, D309A, T310S, S478T and H480Q mutants, which might be a result of the contribution of multiple amino acids to the binding of DBF.

The beta-4 sheet of aromatase, particularly residues S478 and H480, also plays an important role in the binding of coumestrol to aromatase. Mutagenesis study showed that the S478T and H480Q mutants had dramatic effects on the binding of coumestrol to aromatase, which is supported by the current model of the aromatase–coumestrol complex showing close contacts between coumestrol and the S478 and H480 residues. Similar to E2, the planar A ring of coumestrol might have weaker interaction with the beta-4 sheet, when compared to the non-aromatic six-carbon A ring of substrate. This weak interaction with the beta-4 sheet might account for the low binding affinity of coumestrol. Planar flavones in previous studies were shown to have low binding affinity to aromatase [23], which supports the hypothesis that planar phytoestrogens bind to aromatase with lower affinity than the physiological androgen substrates. Phytoestrogen derivative with substitution at the planar rings can increase its binding affinity to aromatase. For example, we have found that 4-benzyl-3-(4′-chlorophenyl)-7-methoxycoumarin is a potent competitive

inhibitor of aromatase with respect to the androgen substrate, having a K_i value of 84 nM [35].

In conclusion, we address the molecular basis for the interaction of aromatase and four different classes of substrates and inhibitors with their own unique structural features. Site-directed mutagenesis experiments provide useful information on determining the orientation of ligands in the docking models and evaluating the predicted active site pocket of aromatase. Conversely, the docking models explain most of the experimental data. These studies demonstrate that the beta-4 sheet plays important role in the binding of different ligands, which supports our previous studies [15] about the predicted active site pocket of aromatase and the clamping mechanism for ligand binding.

Acknowledgments

This work was supported by grants from the California Breast Cancer Research Program [11GB-0125 (YH)] and National Institutes of Health [CA44735 (SC), ES08528 (SC), and CA33572 (the City of Hope Cancer Center grant)].

REFERENCES

[1] Plourde PV, Dyroff M, Dowsett M, Demers L, Yates R, Webster A. ARIMIDEX: a new oral, once-a-day aromatase inhibitor. J Steroid Biochem Mol Biol 1995;53(1–6): 175–9.
[2] Lipton A, Demers LM, Harvey HA, Kambic KB, Grossberg H, Brady C, et al. Letrozole (CGS 20267). A phase I study of a new potent oral aromatase inhibitor of breast cancer. Cancer 1995;75(8):2132–8.
[3] Evans TR, Di Salle E, Ornati G, Lassus M, Benedetti MS, Pianezzola E, et al. Phase I and endocrine study of exemestane (FCE 24304), a new aromatase inhibitor, in postmenopausal women. Cancer Res 1992;52(21):5933–9.
[4] Goss PE, Ingle JN, Martino S, Robert NJ, Muss HB, Piccart MJ, et al. A randomized trial of letrozole in postmenopausal women after five years of tamoxifen therapy for early-stage breast cancer. N Engl J Med 2003;349(19):1793–802.
[5] Coombes RC, Hall E, Gibson LJ, Paridaens R, Jassem J, Delozier T, et al. A randomized trial of exemestane after two to three years of tamoxifen therapy in postmenopausal women with primary breast cancer. N Engl J Med 2004;350(11):1081–92.
[6] Baum M, Budzar AU, Cuzick J, Forbes J, Houghton JH, Klijn JG, et al. Anastrozole alone or in combination with tamoxifen versus tamoxifen alone for adjuvant treatment of postmenopausal women with early breast cancer: first results of the ATAC randomised trial. Lancet 2002;359(9324):2131–9.
[7] Nabholtz JM, Buzdar A, Pollak M, Harwin W, Burton G, Mangalik A, et al. Anastrozole is superior to tamoxifen as first-line therapy for advanced breast cancer in postmenopausal women: results of a North American multicenter randomized trial. Arimidex Study Group. J Clin Oncol 2000;18(22):3758–67.
[8] Graham-Lorence S, Amarneh B, White RE, Peterson JA, Simpson ER. A three-dimensional model of aromatase cytochrome P450. Protein Sci 1995;4(6):1065–80.
[9] Auvray P, Nativelle C, Bureau R, Dallemagne P, Seralini GE, Sourdaine P. Study of substrate specificity of human aromatase by site directed mutagenesis. Eur J Biochem 2002;269(5):1393–405.
[10] Chen S, Zhang F, Sherman MA, Kijima I, Cho M, Yuan YC, et al. Structure–function studies of aromatase and its inhibitors: a progress report. J Steroid Biochem Mol Biol 2003;86(3–5):231–7.
[11] Kao YC, Korzekwa KR, Laughton CA, Chen S. Evaluation of the mechanism of aromatase cytochrome P450. A site-directed mutagenesis study. Eur J Biochem 2001;268(2): 243–51.
[12] Chen S, Kao YC, Laughton CA. Binding characteristics of aromatase inhibitors and phytoestrogens to human aromatase. J Steroid Biochem Mol Biol 1997;61(3–6): 107–15.
[13] Kao YC, Cam LL, Laughton CA, Zhou D, Chen S. Binding characteristics of seven inhibitors of human aromatase: a site-directed mutagenesis study. Cancer Res 1996;56(15):3451–60.
[14] Favia AD, Cavalli A, Masetti M, Carotti A, Recanatini M. Three-dimensional model of the human aromatase enzyme and density functional parameterization of the iron-containing protoporphyrin IX for a molecular dynamics study of heme-cysteinato cytochromes. Proteins 2006;62(4):1074–87.
[15] Hong Y, Yu B, Sherman M, Yuan YC, Zhou D, Chen S. Molecular basis for the aromatization reaction and exemestane-mediated irreversible inhibition of human aromatase. Mol Endocrinol 2007;21(2):401–14.
[16] Hornung MW, Jensen KM, Korte JJ, Kahl MD, Durhan EJ, Denny JS, et al. Mechanistic basis for estrogenic effects in fathead minnow (Pimephales promelas) following exposure to the androgen 17alpha-methyltestosterone: conversion of 17alpha-methyltestosterone to 17alpha-methylestradiol. Aquat Toxicol 2004;66(1):15–23.
[17] Miller VP, Streser D, Crespi CL. Use of fluorescein aryl ethers in high throughput cytochrome P450 inhibition assays. United States Patent US 6,420,131 B1; 2002.
[18] Wang C, Makela T, Hase T, Adlercreutz H, Kurzer MS. Lignans and flavonoids inhibit aromatase enzyme in human preadipocytes. J Steroid Biochem Mol Biol 1994;50(3–4):205–12.
[19] Zhou DPD, Chen S. Stable expression of human aromatase complementary DNA in mammalian cells: a useful system for aromatase inhibitor screening. Cancer Res 1990;50:6949–54.
[20] Zhou DJ, Pompon D, Chen SA. Stable expression of human aromatase complementary DNA in mammalian cells: a useful system for aromatase inhibitor screening. Cancer Res 1990;50(21):6949–54.
[21] Zhang F, Zhou D, Kao YC, Ye J, Chen S. Expression and purification of a recombinant form of human aromatase from Escherichia coli. Biochem Pharmacol 2002;64(9): 1317–24.
[22] Bradford MM. A rapid and sensitive method for the quantitation of microgram quantities of protein utilizing the principle of protein-dye binding. Anal Biochem 1976;72:248–54.
[23] Kao YC, Zhou C, Sherman M, Laughton CA, Chen S. Molecular basis of the inhibition of human aromatase (estrogen synthetase) by flavone and isoflavone phytoestrogens: A site-directed mutagenesis study. Environ Health Perspect 1998;106(2):85–92.
[24] Philpot RM, Hodgson E. Differences in the cytochrome P-450S from resistant and susceptible house flies. Chem Biol Interact 1972;4(6):399–408.
[25] Tate LG, Plapp FW, Hodgson E. Cytochrome P-450 difference spectra of microsomes from several insecticide-resistant and -susceptible strains of the housefly, Musca domestica L.. Chem Biol Interact 1973;6(4):237–47.

[26] Mor G, Eliza M, Song J, Wiita B, Chen S, Naftolin F. 17alpha-methyl testosterone is a competitive inhibitor of aromatase activity in Jar choriocarcinoma cells and macrophage-like THP-1 cells in culture. J Steroid Biochem Mol Biol 2001;79(1–5):239–46.
[27] Trosken ER, Fischer K, Volkel W, Lutz WK. Inhibition of human CYP19 by azoles used as antifungal agents and aromatase inhibitors, using a new LC-MS/MS method for the analysis of estradiol product formation. Toxicology 2006;219(1–3):33–40.
[28] Keizers PH, Schraven LH, de Graaf C, Hidestrand M, Ingelman-Sundberg M, van Dijk BR, et al. Role of the conserved threonine 309 in mechanism of oxidation by cytochrome P450 2D6. Biochem Biophys Res Commun 2005;338(2):1065–74.
[29] Dahl AR, Hodgson E. The interaction of aliphatic analogs of methylene-dioxyphenyl compounds with cytochromes P-450 and P-420. Chem Biol Interact 1979;27(2–3):163–75.
[30] Schalk M, Cabello-Hurtado F, Pierrel MA, Atanossova R, Saindrenan P, Werck-Reichhart D. Piperonylic acid, a selective, mechanism-based inactivator of the trans-cinnamate 4-hydroxylase: a new tool to control the flux of metabolites in the phenylpropanoid pathway. Plant Physiol 1998;118(1):209–18.
[31] Marcus CB, Murray M, Wilkinson CF. Spectral and inhibitory interactions of methylenedioxyphenyl and related compounds with purified isozymes of cytochrome P-450. Xenobiotica 1985;15(4):351–62.
[32] Grubb MF, Diamond S, Christ DD. In vitro and in vivo effects of the arylamine human immunodeficiency virus protease inhibitor 4R-(4alpha,5alpha,6beta, 7beta)-1-[(3-(1-imidazoylcarbamoyl)phenyl)methyl]-3-[(3-aminophenyl)methyl]hexahydro-5,6-dihydroxy-4,7-bis(phenylmethyl)-2H-1,3-diazepin-2-one (SD894) on rat hepatic cytochrome P450 2B and 3A. Drug Metab Dispos 1997;25(12):1424–8.
[33] Franklin MR. Methylenedioxyphenyl insecticide synergists as potential human health hazards. Environ Health Perspect 1976;14:29–37.
[34] Pessayre D, Descatoire V, Konstantinova-Mitcheva M, Wandscheer JC, Cobert B, Level R, et al. Self-induction by triacetyloleandomycin of its own transformation into a metabolite forming a stable 456 nm-absorbing complex with cytochrome P-450. Biochem Pharmacol 1981;30(6):553–8.
[35] Chen S, Cho M, Karlsberg K, Zhou D, Yuan YC. Biochemical and biological characterization of a novel anti-aromatase coumarin derivative. J Biol Chem 2004;279(46):48071–8.